Estuarine, Coastal and Shelf Science 204 (2018) 212–224

Contents lists available at ScienceDirect

Estuarine, Coastal and Shelf Science

journal homepage: www.elsevier.com/locate/ecss

Suspended particle dynamics and fluxes in an Arctic fjord (Kongsfjorden, Svalbard)

Florian Meslard [a, b], François Bourrin [a, b, *], Gaël Many [a, b, c], Philippe Kerhervé [a, b]

[a] Université Perpignan Via Domitia, CEntre de Formation et de Recherche sur les Environnements Méditerranéens, UMR 5110, F-66860, Perpignan, France
[b] CNRS, Centre de Formation et de Recherche sur les Environnements Méditerranéens, UMR 5110, F-66860, Perpignan, France
[c] Service Hydrographique et Océanographique de la Marine, CS 92803, 29228, Brest, France

ARTICLE INFO

Article history:
Received 7 July 2017
Received in revised form
19 February 2018
Accepted 19 February 2018
Available online 2 March 2018

ABSTRACT

An experiment was carried out during summer 2015 in the inner part of the Kongsfjorden to study the inputs of meltwater and behaviour of associated suspended particles. We used a wide range of oceanographic instruments to assess the hydrological and hydrodynamic characteristics of coastal waters. The transfer of suspended particles occurs from a large surface plume fed by two main sources: the most important one is the upwelling of fresh and turbid water coming from a tide-water glacier: the Kronebreen, and the second one from a continental glacier: the Kongsvegen. We estimated that these two sources discharged about $2.48 \pm 0.37 \times 10^6$ t of suspended sediments during the two months of melting. The major part of these sediments is deposited within the first kilometre due to flocculation phenomena. Flocculation is initiated below the surface turbid plume and is mainly caused by the salinity gradient and high suspended particle concentration. Finally, our estimates of suspended particle fluxes by a typical Arctic coastal glacier showed the need to consider suspended sediment fluxes from high-latitude areas into global budgets in the context of climate change.

© 2018 Elsevier Ltd. All rights reserved.

1. Introduction

Long-term measurements suggest that the Arctic is the region of the northern hemisphere where warming has enhanced the fastest modifications over the past few decades (Serreze and Barry, 2011). These changes are often observed in the form of rainfall increase, melting of the permafrost, decrease in snow cover and ice, as well as an increase in river flows and sea level rise. All these changes have led to the increase of freshwater inputs into the Arctic Ocean, combined with particulate (mostly sediments) and dissolved material inputs, which have induced a deep evolution in its hydrologic, sedimentary and biogeochemical functioning (ACIA, 2004). These enhanced transfers, from land to sea, are believed to be principally driven by large Arctic rivers, such as the Mackenzie River or the Lena River, which discharge about 4200 km^3 of freshwater and 221×10^6 t of sediments annually (AMAP, 1997). Nonetheless, glaciers, which represent an ice stock of about 3×10^6 km^3 for the entire Arctic region (Coupel et al., 2012), largely contribute during the summer to these inputs of melting freshwater (about 400 km^3 for Greenland's glaciers) and associated sediments (Bamber et al., 2012; Barnes et al., 1982; Mernild and Hasholt, 2009). It has been well documented that exported dissolved and particulate materials from glaciers may affect primary production (Calleja et al., 2017; Piwosz et al., 2009) as well as pelagic-benthic coupling (Bourgeois et al., 2016). Moreover, coastal glaciers have been mostly investigated by glaciologists and hydrologists, who mainly estimated water and suspended sediment fluxes from measurements in the continental part of the glacier (Mernild and Hasholt, 2009). Few studies have focussed on the behaviour of these inputs into the coastal area based on in-situ measurements of water properties and suspended particle characteristics (Lund-Hansen et al., 2010).

Sediment inputs from coastal glaciers mostly occur during the summer melting season, which is limited to a few months. Hodson et al. (1998) estimated that the average melting period is about 60 days in Svalbard. Discharge and suspended sediment load by glaciers were shown to be strongly dependant on the accumulated number of positive-degree days (Mernild and Hasholt, 2009). These inputs can generate important low-saline and turbid plumes that cause high stratification in coastal fjord waters (Hop et al., 2002).

* Corresponding author. Université Perpignan Via Domitia, CEntre de Formation et de Recherche sur les Environnements Méditerranéens, UMR 5110, F-66860, Perpignan, France.
E-mail address: fbourrin@univ-perp.fr (F. Bourrin).

https://doi.org/10.1016/j.ecss.2018.02.020
0272-7714/© 2018 Elsevier Ltd. All rights reserved.

These sediment-laden plumes spread and settle down along fjords and on adjacent shelves depending on local hydrodynamic regimes. These processes are strongly dependant on particle size, nature, effective density, and their capacity to form aggregates or flocs (Nittrouer et al., 2009; Simpson and Sharples, 2012). Indeed, particles can clump together and form bigger particles with higher settling velocities. This flocculation process generally occurs at the interface between fresh and salt water. While aggregation phenomena require biogenic organic matter and generally occur further offshore (Nittrouer et al., 2009; Syvitski, 1989), the flocculation process is strongly controlled by the suspended particulate matter (SPM) concentration, the turbulence (Manning and Schoellhamer, 2013; Safak et al., 2013), as well as the salinity gradient (Dagg et al., 2004). The flocculation process has largely been described in temperate estuaries where it controls the dynamics of fine particles, but the role of flocculation/aggregation phenomena in glacial environments is poorly documented.

The aim of this study is to investigate the dynamics, the evolution, and the transformation of suspended particles entering a typical Arctic fjord (the Kongsfjorden, Svalbard) through the melting freshwater of a coastal glacier. We first describe the characteristics of the inner-fjord of the Kongsfjorden, in terms of hydrology, hydrodynamics, and distribution of suspended particle. Then, we investigate the characteristics of in situ suspended particles and their transfer mechanisms from their sources (glacier front) towards the inner-fjord. Finally, we attempt to estimate suspended sediment fluxes coming from melting freshwater in this Arctic system and compare them to other similar Arctic and temperate coastal systems.

2. Regional settings

Svalbard is a Norwegian archipelago composed of more than 30 islands located at the limit between the Arctic Ocean and the North Atlantic, approximately 500 km east of Greenland (Fig. 1a). The largest of these islands, Spitsbergen, presents on its northwest coast a two-armed fjord system, the Kongsfjorden-Krossfjorden (Fig. 1b). Kongsfjorden (Fig. 1c) is located to the south of this system, and is a glacial eroded fjord oriented from south-east to northwest (between 78°50′N, 11°20′E and 79°50′N, 12°38′E) extending over a length of 20 km and a width of 4 – 10 km (Maclachlan et al., 2010). Covering a total area of 208.8 km^2 and filling a total volume of 29.4 km^3 (Ito and Kudoh, 1997), it is surrounded by several terrestrial glaciers and 5 tidewater glaciers: Blomstrandbreen, Conwaybreen, Kongsbreen, Kronebreen, and Kongsvegen. These glaciers strongly influence the fjord hydrology, bringing each year about 1 km^3 of freshwater to the fjord, with a seasonal peak in summer (Lefauconnier et al., 1999). These inputs create large turbid plumes highly visible from satellites (Fig. 1c). These fresh and turbid water inputs induce strong physical gradients of temperature, salinity and SPM concentrations between coastal and offshore waters (Hop et al., 2002). The circulation in the fjord was often described as a two-layer system with a bottom layer mainly influenced by the intrusion of water masses from the shelf, and a surface layer controlled by the microtidal regime, glacial runoff and local winds (Ingvaldsen et al., 2001; Svendsen et al., 2002).

Kongsfjorden is divided into an outer and central basin with maximum water depths ranging between 200 and 400 m and a well-marked inner basin with shallow water depths lower than 100 m (Elverhøi et al., 1983; Howe et al., 2003). This shallow basin, which extends over 10 km from the ice front, is the most dynamic zone of Kongsfjorden because of the influence of glacial melting freshwaters. This area corresponds to the proximal zone and presents the largest glacier front of the Kongsfjorden formed by the merging of Kronebreen, Kongsvegen and Infantfonna glaciers. Kronebreen is one of the biggest glaciers of Svalbard with a surface area of 406.9 km^2 (Blaszczyk et al., 2009), and presents the highest surface velocities ranging from 750 to 785 $m\,y^{-1}$ (Bennett et al., 1999; Lefauconnier et al., 1994; Melvold and Hagen, 1998). This ice flow towards the fjord induces an annual ice loss by calving of 0.25 km^3 (Lefauconnier et al., 1994). Kongsvegen covers an area of 153.9 km^2 and presents a surface velocity of only 1.4 – 3.6 $m\,y^{-1}$ with a low annual ice loss of 4×10^{-4} km^3 (Blaszczyk et al., 2009). Contrary to Kronebreen, Kongsvegen started to emerge from tidewater between 1990 and 2005 after the gradual building of an ice-contact delta (Trusel et al., 2010).

3. Materials and methods

All samples and data were collected in the Kongsfjorden between 20 July and 3 August 2015 by using the coastal vessels “Jean Floc'h” from AWIPEV and “Teisten” from Kings Bay AS. Several sampling and measurement stations, as well as ADCP transects, were performed to characterise the turbid plumes resulting from meltwater discharges along the Kronebreen-Kongsvegen front (Fig. 1c). At each station, an in-situ instrumental package was deployed to monitor the hydrological parameters and the suspended particle characteristics. Water samples and sediment traps were also collected for further analyses (see hereafter).

3.1. Meteorological and tidal conditions

Hourly data of air temperature, wind speed and direction were obtained at the Ny-Ålesund station from the meteorological and radiation data of the AWIPEV research base. The air temperature was measured at 2 m height above solid ground using a PT-100 resistance thermometer. Wind speed and direction were measured using a Thies Clima combined wind sensor installed at 10 m height above solid ground (Maturilli et al., 2013).

Hourly water level measurements were obtained from the Norwegian Hydrographic Service at the Ny-Ålesund station. The water level was measured from the Chart Datum reference level ($Z_O = 92.2$ cm).

3.2. Hydrology and hydrodynamics

A Seabird SBE 19-plus CTD (Conductivity-Temperature-Depth) with an acquisition frequency of 4 Hz was deployed at 11 stations along the ice front (black dots in Fig. 1c) and across the inner-fjord (yellow dots in Fig. 1c). Derived parameters such as salinity and seawater density sigma-t were calculated using the EOS-80 algorithms (UNESCO, 1983) and SBE Data Processing® software. Turbidity was simultaneously measured using a Seapoint Turbidity Meter (880 nm). Because of high SPM concentrations, data above 130 $mg\,L^{-1}$ were not used due to sensor saturation. Measurement corrections such as conductivity and cell thermal mass were processed using manufacturer recommendations. Data were smoothed using a median filter with a window size of 10 points, and binned into intervals of 0.5 m.

A 300 kHz RDI BB ADCP (Broad Band Acoustic Doppler Current Profiler) towed on the side of the boat was used to identify the hydrodynamic properties of the water column. Current magnitude and direction were measured in depth cells of 1 m with a range of 100 m using high rate pinging mode. A total of 17 ADCP transects were carried out in the proximal area of the fjord from 20 July to 3 August 2015. North-South transects were performed to describe the structure of freshwater sources along the ice front, while South-East - North-West transects were performed across the proximal zone to characterise the behaviour of the freshwater plumes inside the inner part of the fjord (selected transects are indicated with

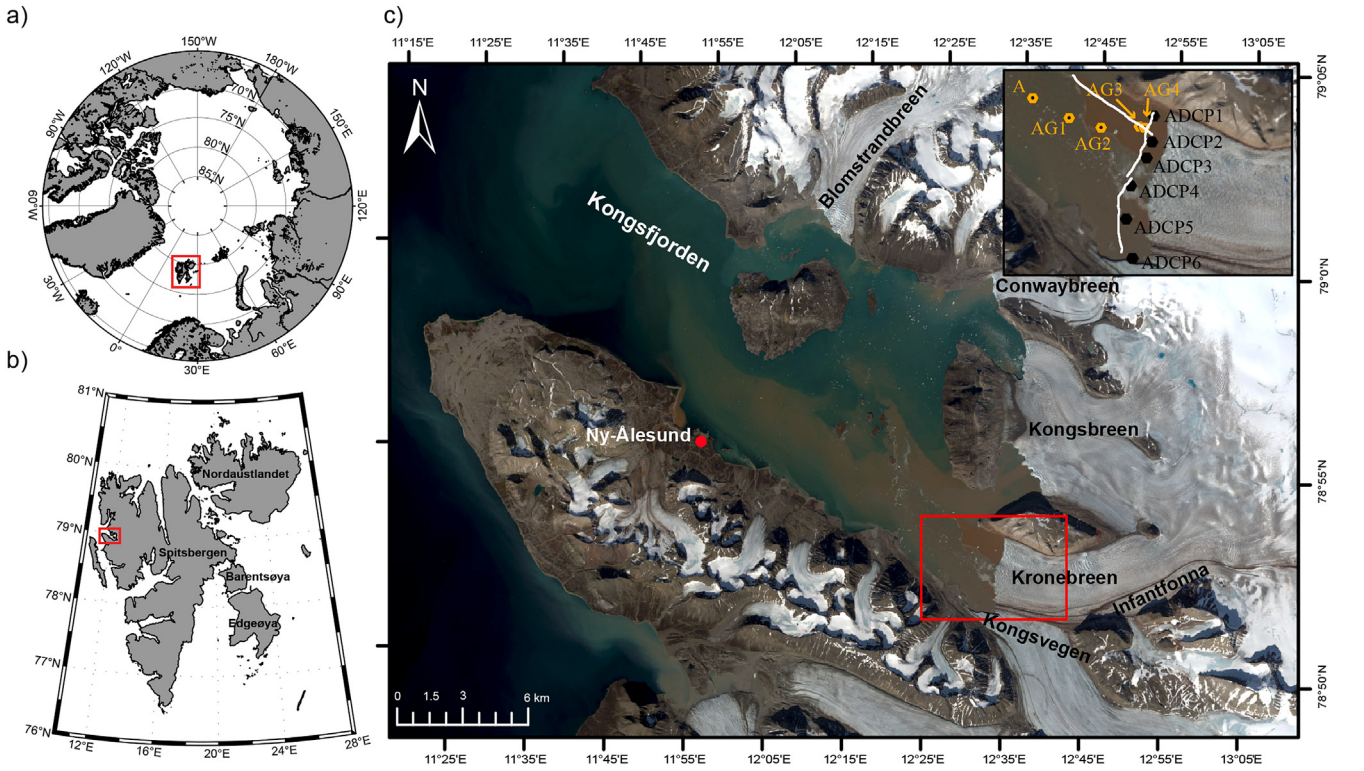

Fig. 1. a) Map of the Arctic Ocean showing the localisation of Svalbard in the red square. b) Map of Svalbard indicating the position of Kongsfjorden in the red square. c) Landat 8 image measured on 1st August 2015 including the position of sampling stations. The red square corresponds to a zoom on the ice front in the upper right portion of the figure. Sampling stations are indicated by black and yellow dots. Selected ADCP transects are indicated by white lines. The N-S transect is composed of 2 sections (northern and southern). (For interpretation of the references to colour in this figure legend, the reader is referred to the Web version of this article.)

white lines in Fig. 1c). High-resolution bottom tracking was used to estimate the bathymetry and water velocity magnitude and direction using WinRiver II® software. The first 2 m were not monitored due to the depth of the transducers (≈50 cm) and the ADCP blanking distance. Furthermore, the last 10 m were not used due to contamination between primary and secondary lobes. Finally, these data were averaged over periods of 30 s. Transects were georeferenced using GPS fixes acquired during the deployment.

All ADCP transects performed during the investigated period showed the same pattern in terms of surface current. Then, a map of surface current magnitude and direction was processed using all the ADCP transects covering the proximal area of the fjord. The DIVA (Data-Interpolating Variational Analysis) gridding method was used to interpolate data over a regular grid.

3.3. Sampling of SPM

Water samples were collected using a 10 L Niskin bottle. The sampling bottle was located 1 m vertically above the instrument package. Samples were taken at 5, 10, 20, 30 m depth and 3 m above the seabed. Between 195 mL and 3 L of seawater were filtered in triplicates on pre-weighed 0.7 μm GF/F Whatman filters, depending on turbidity. Then, the filters were rinsed with deionized water, dried at 50 °C and re-weighed. The data were averaged to determine the absolute mass concentration of SPM and uncertainties in the measurements in mg L^{-1}.

Cylindrical sediment traps consisting of four tubes mounted on a gimballed frame (KC Denmark) were deployed at the station A (85 m depth, Fig. 1c) at 30 m above the bottom. The settled material was collected every 2–5 days and used for further grain-size analysis (see above) to allow comparison with in-situ grain-size measurements.

3.4. SPM characterisation

3.4.1. Laser diffraction

A Sequoia Scientific Inc. LISST-100X type C was used to estimate the in-situ particle size distribution (PSD) and the attenuation coefficient c at 660 nm. An optical reduction path module (RPM) of 90% was used due to high in-situ turbidity. Data were collected at 10 Hz and averaged in 10-value bursts. The PSD was derived from the laser diffraction spectrum after mathematical inversion using a "randomly shaped" model resolving the Mie theory (Agrawal et al., 2008; Agrawal and Pottsmith, 2000). The PSD data consisted of volume distributions of the particles in 32 logarithmically spaced classes ranging from 2.5 to 500 μm. Each size class characterised a volume concentration (expressed in μL L^{-1}) obtained using the factory volume calibration constant and subtracting a background. As the accuracy of measurements in the extreme size classes of the LISST was highly variable (Traykovski et al., 1999), corresponding fine (<2.95 μm) and large particles (>304 μm) were considered outside of the instrument measurement range and were removed (Mikkelsen et al., 2005). The total volume concentration was then calculated from the resulting PSD.

Unlike the in-situ PSD, the determination of the primary PSD of the SPM and trapped particles were carried out on sonicated (deflocculated) samples with a laboratory Malvern Mastersizer 3000. The estimate of PSD was also made using the Mie theory and used to describe suspended particles between 0.1 and 1000 μm. Each sample was measured five times and the data were then averaged.

3.4.2. Optical and acoustic signal calibration

The attenuation coefficient c (660 nm) from the LISST-100X instrument was used to derive the SPM concentrations from in-situ

SPM measurements. To improve the calibration, data were binned in classes of 10 m^{-1}. Finally, we used an ordinary least squares regression method through the origin ($R^2 = 0.94$, n = 22) and found the following relationship between SPM concentration and the attenuation coefficient (Fig. 2a):

$$[SPM]_{opt}\ (mg\ L^{-1}) = 1.5951\ (\pm\ 0.11) \times c\ (660\ nm)\ (m^{-1}) \quad (1)$$

Then, we used the Echo Intensity (EI) from ADCP measurements and $[SPM]_{opt}$ (equation (1)) to estimate SPM concentrations. EI, which depends on transmitted power, sound absorption, beam spreading and backscatter coefficient, is a measurement of the intensity of the returning echo from the transducers. The Backscatter Index (BI) was obtained from Winriver II® software applying corrections to the EI for water absorption, geometrical spreading, particle attenuation, and count-to-dB conversion. BI was then linked to SPM concentration based on equation (2):

$$10\log_{10}[SPM]_{opt} = A \times BI + B \quad (2)$$

Where $[SPM]_{opt}$ is the SPM concentration derived from equation (1), A is the slope, BI the backscatter index, and B the intercept.

Due to the presence of icebergs, the two measurements were not performed at exactly the same locations. We therefore performed an objective analysis to match the acoustic data with the nearest calibrated optical data. Data quality was checked using the correlation between acoustic beams. Then we used an ordinary least squares regression ($R^2 = 0.97$, n = 39) between the backscatter index and SPM concentration via the following equation (Fig. 2b)

$$[SPM]_{acoust}\ (mg\ L^{-1}) = 10^{((0.741\ (\pm 0.02) \times BI\ -48.918\ (\pm 1.92))\ /\ 10)} \quad (3)$$

3.4.3. Effective density

The effective density ($\Delta\rho$ in kg m^{-3}) of the particle assemblage was calculated with SPM concentrations ($[SPM]_{opt}$ in mg L^{-1}) and total volume concentration (VC_{tot} in µl L^{-1}) obtained by summing all the particle volume concentrations from each size class ($C_{vol,\ i}$) according to the equations:

$$VC_{tot} = \sum C_{vol,i} \quad (4)$$

$$\Delta\rho = [SPM]_{opt}\ /\ VC_{tot} \quad (5)$$

For the calculation of $\Delta\rho$, the 32 classes measured by the LISST-100X were considered to match with attenuation coefficient used in the calculation of the SPM concentrations.

3.4.4. Suspended particulate fluxes

To estimate water and SPM fluxes originating from the Kronebreen-Kongsvegen complex, we used 2 combined ADCP transects performed along the ice front (Fig. 1c). EI data were used to derive SPM concentrations following the above method. Current velocities and directions were converted into north and east components. Then, SPM concentrations were multiplied by the east component (i.e., the cross-ice front component) over the measured area, providing an instantaneous SPM flux in g s^{-1} for each ADCP measurement cell. Finally, all individual fluxes were summed over the whole investigated cross-section to estimate instantaneous fluxes and the result was multiplied by the mean number of days during the melting season to obtain a rough estimate of the annual flux of water and sediments. We extracted the accumulated number of days where the daily average air temperature was superior to 5 °C from meteorological time-series measured in Ny-Ålesund in 2015. The obtained value of 60 days matches the mean number of days of the melting season in Svalbard (Hodson et al., 1998). Uncertainties in water and SPM flux estimates were obtained by considering the errors in the current magnitude and direction measurements, and errors in the acoustically derived SPM concentrations.

4. Results

4.1. Meteorological and tidal conditions

From 20 July to 3 August, we observed two different wind regimes (Fig. 3a). From 22 to 26 July, a north-westerly wind was

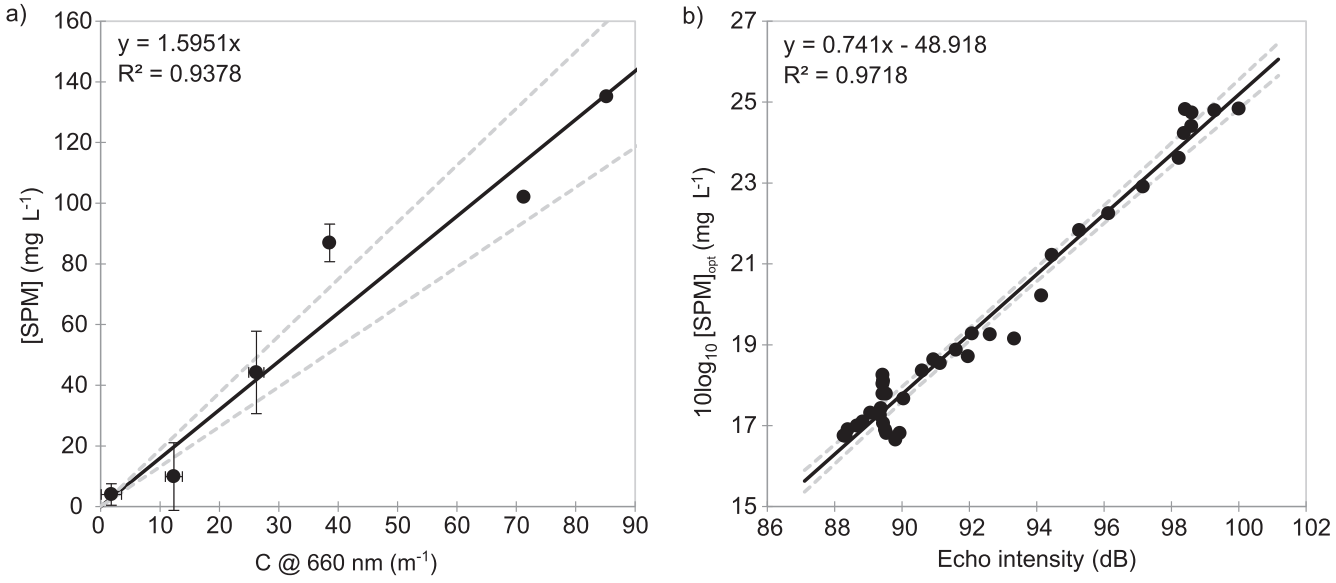

Fig. 2. a) Calibration curve of the attenuation coefficient c (660nm) of the LISST-100X vs in-situ SPM measurements. The standard deviation of each group is shown. Dashed lines represent the 95 % confidence interval of the regression. b) Calibration curve of the Echo Intensity (EI) of the ADCP vs optically derived SPM concentrations. Dashed lines represent the 95 % confidence interval of the regression.

dominant with a maximum wind speed of 9.6 m s^{-1}. From 2 July to 3 August a south-easterly wind was dominant with a maximum wind speed of 7.6 m s^{-1}. The minimum tidal amplitude was reached on 27 July with a range of 60 cm during the neap tide. The maxium tidal amplitude was reached on 3 August with a range of 120 cm (Fig. 3b). Air temperature varied from 2.75 °C on 25 July to 14.93 °C on 2 August (Fig. 3c).

4.2. Hydrology

Fig. 4a shows the hydrological structures measured on 31 July 2015. An important stratification of the water column was observed throughout the 3-km long transect perpendicular to the glacier front. The surface layer was 20 m thick and presented temperatures lower than 3 °C as well as low salinities ranging from 27 to 33. Corresponding densities ranged from 23 to 27 kg m^{-3}. These surface waters were characterised by maximum SPM concentrations around 300 mg L^{-1} close to the glacier (station AG3). These high concentrations rapidly decreased to reach 140 mg L^{-1} 2.5 km away from the ice front (station A). Below the surface layer, the water column was homogenous with salinities between 26 and 27, densities from 27 to 29 kg m^{-3}, and SPM concentrations lower than 40 mg L^{-1}. However, temperatures exhibited the highest values (from 3.5 to 4.5 °C) below the surface layer (between 20 and 50 m depth) before rapidly decreasing to 1 °C at 70 m depth.

Hydrological structures along the Kronebreen-Kongsvegen ice complex (Fig. 4b) were measured on 3 August 2015. An important stratification of the water column was again visible with a vertical front at km 1 between stations ADCP2 and ADCP3. This front delimited the end of a surface layer about 4 m thick, spreading from stations ADCP3 to ADCP6. In this surface layer, salinities ranged from 24 to 31, densities from 22 to 26 kg m^{-3}, temperatures were lower than 2 °C, whereas SPM concentrations varied from 200 mg L^{-1} close to station ADCP6 to 80 mg L^{-1} close to station ADCP5. On the northern part of the transect, maximum SPM concentrations reached up to 300 mg L^{-1} in the subsurface (10 m depth) between stations ADCP1 and ADCP2. This turbid layer was associated with salinities ranging from 30 to 33, densities from 24 to 26 kg m^{-3} and temperatures were below 3.5 °C. Below the surface layer, the water column was rather homogenous with salinities between 33 and 34.5, densities between 26 and 27.5 kg m^{-3}, and SPM concentrations were lower than 40 mg L^{-1}. Below 20 m depth, water temperatures highlighted stratified layers with high temperatures (from 3.5 to 5 °C) between 15 and 40 m depth and low temperatures (below 2 °C) around 40 m depth.

4.3. Hydrodynamics

4.3.1. Subsurface currents

The map of current vectors at 3 m depth (Fig. 5) shows that the

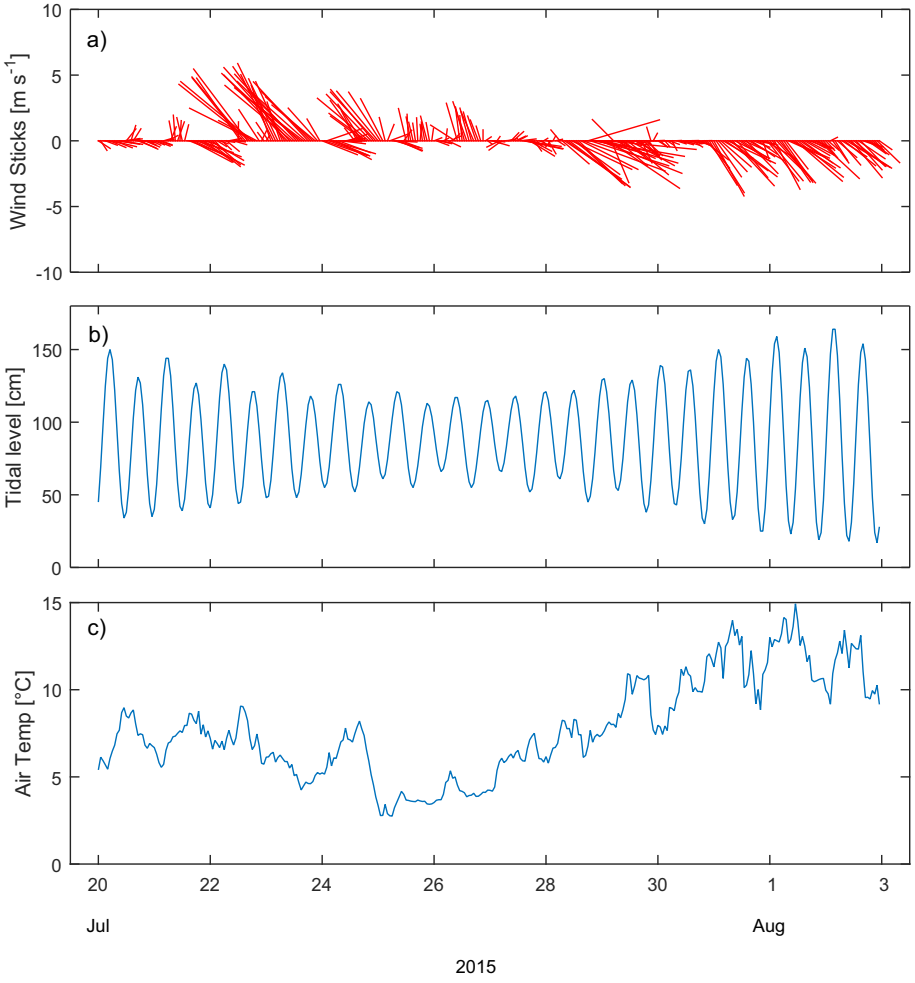

Fig. 3. From top to bottom: a) stick plot of wind speed and direction (by convention the stick plot indicates the direction from where the wind is blowing), b) tidal level and c) air temperature measured in Ny-Ålesund.

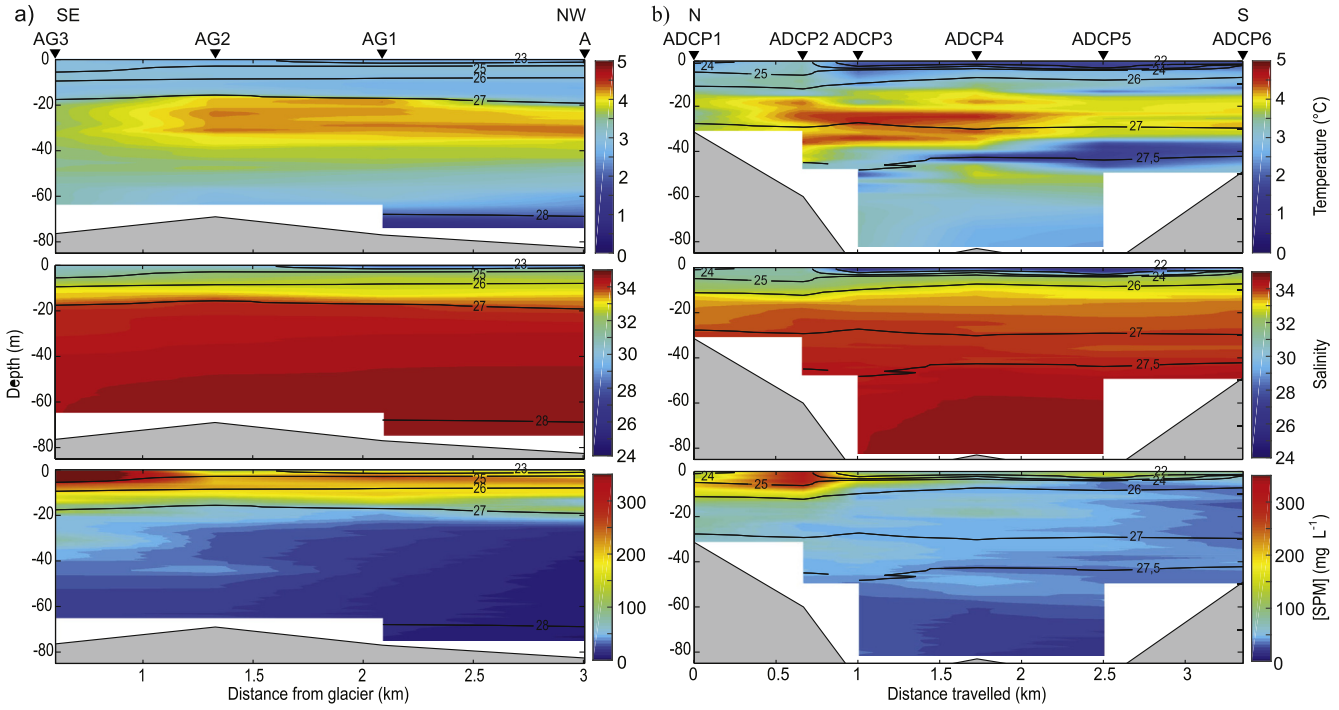

Fig. 4. a) SE-NW hydrological transect from CTD measurements on 31 July 2015. b) N-S hydrological transect parallel to the ice front measured on 3 August 2015. From top to bottom: temperature (°C), salinity and SPM concentrations (mg L^{-1}). Contour lines represent the seawater density (sigma-t in kg m^{-3}). The localisation of stations is indicated in the top plots by black triangles and are also indicated in Fig. 1c with the positionof transects.

strongest currents were measured in the north of the proximal zone and were oriented north-westwards. In this area, we observed maximum velocities higher than 0.3 m s^{-1} with a maximum of 0.5 m s^{-1} close to the Kronebreen ice front. Several cells of strong current velocities were observed from the Kronebreen towards the north-west of the proximal zone. In the southern part of the area, current directions and velocities were highly variable. Indeed, along the southern coast and up to the delta, strong currents oriented toward the ice front were observed with velocities ranging between 0.3 and 0.4 m s^{-1}.

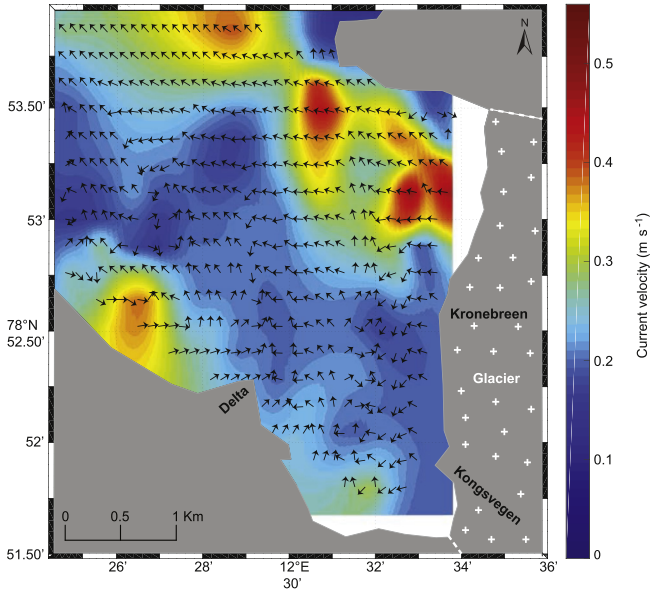

Fig. 5. Map of average current vectors at 3 m depth measured from 20 July to 3 August 2015. Arrows are normalized and indicate in which direction currents were going. A color scale is used to show current velocity (m s^{-1}). (For interpretation of the references to colour in this figure legend, the reader is referred to the Web version of this article.)

4.3.2. *Water column current field*

The SE-NW transect performed on 31 July 2015 shows strong surface currents in the first 10 m below the surface up to 0.4 m s^{-1} oriented westwards (Fig. 6a, bottom panel). Below 10 m water depth, current velocities were lower than 0.2 m s^{-1} and were oriented eastwards toward the fjord. The surface layer was also associated with high SPM concentrations (up to 170 mg L^{-1}) close to the ice front (Fig 6a, top panel). Moreover, SPM concentrations decreased with distance from the glacier with mean values of about 80 mg L^{-1} in the subsurface 2.5 km offshore. The top turbid layer also tends to thicken from 30 m close to the ice front to 1–2 m 2.5 km offshore. Below the surface layer, SPM concentrations were lower than 50 mg L^{-1} except in the vicinity of the ice front where values higher than 50 mg L^{-1} were observed at the bottom.

Acoustically derived SPM concentrations measured along the N-S transect performed on 3 August 2015 (Fig 6b, top panel) show a specific triangular shape with the highest SPM concentrations (up to 350 mg L^{-1}) in the middle of the transect. This turbid structure extended up to 400 m width at the subsurface and occupied the whole water column in its centre. SPM concentrations rapidly decreased to 50 mg L^{-1} at the edges of the structure. Horizontal currents (Fig. 6b, bottom panel) were oriented mainly westwards in the surface layer and showed maximum current velocities of 0.5 m s^{-1} at 3 m depth. Below 10 m depth, currents were mainly oriented eastwards toward the ice front and showed velocities below 0.2 m s^{-1}.

4.4. *SPM characteristics*

In situ PSD and volume concentrations measured by the LISST-

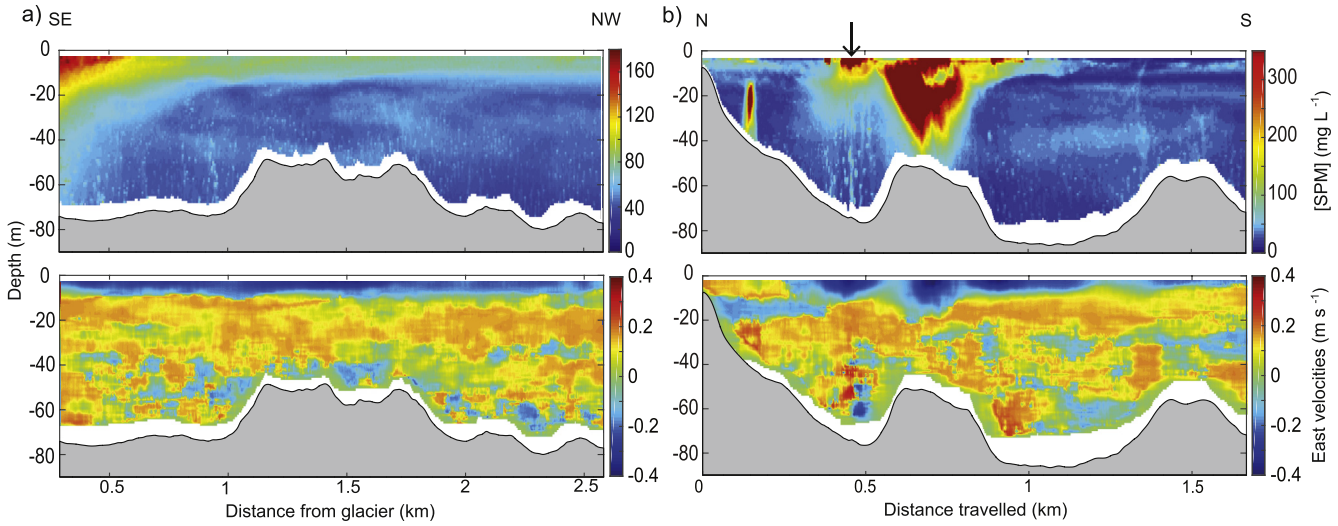

Fig. 6. a) ADCP SE-NW transect measured on 3 August 2015 and b) N-S transect measured on 31 July 2015 (see Fig. 1c for the localisation of transects). From top to bottom: acoustic-derived SPM concentration (in mg L^{-1}) and horizontal current velocities (m s^{-1}). Positive values are eastwards currents and negative values are westwards currents. Note the different colorbar scales for SPM concentration for both transects. The position of the SE-NW transect (Fig. 6a) is indicated by the arrow above the N-S transect (Fig. 6b). (For interpretation of the references to colour in this figure legend, the reader is referred to the Web version of this article.)

100X on 28 July 2015 are presented in Fig. 7 from the glacier front (station AG4) to the fjord (station AG1) at different water depths. Mean PSD of primary particles were determined in the laboratory from water and sediment trap samples (station A) after ultrasonification.

4.4.1. Primary PSD

Primary PSD measured from in-situ water samples and from sediment traps showed the same distribution (Fig. 7a). Primary PSD showed two principal modes: one centred around 6–10 μm, corresponding to fine silts or very fine silts, and the other centred around 0.7–1 μm, corresponding to clays. Silty and clayey fractions represented 74% and 25% of the primary particles PSD, respectively. In-situ PSD generally showed larger particles than the PSD of corresponding primary particles at all sampling stations and depths.

4.4.2. In situ PSD

As already observed for the SPM mass concentrations, the volume concentrations also decreased with distance from the glacier in the surface layer (Fig. 7a) and with water depth at all stations (Fig. 7). Indeed, volume concentrations decreased from 116.93 μL L^{-1} at station AG4 to 14.98 μL L^{-1} at station AG1 (from 0.38 to 2.1 km from the ice front). At all sampling stations, the PSD of surface waters was characterised by fine silts (main modes between 6 and 15 μm). Moreover, we observed coarser particles with increasing depths (i.e., main modes from 6 μm at the surface to 80 μm at 30 m depth at station AG4 close to the glacier front) and at the proximity of the glacier front (i.e., at 20 m depth main modes from 20 μm at station AG1 to 60 μm at station AG4 close to the glacier front). Whereas the finest particles were measured in the surface waters, the coarsest particles were measured close to the ice front at 30 m water depth with main modes around 75–90 μm (station AG4). Close to the seabed, PSD at all stations were characterised by finer particles mainly composed of silts.

In situ particle assemblage properties (VC_{tot}, SPM concentrations and effective densities) are summarized in Table 1. Effective densities roughly decreased with the distance from the glacier, as well as with the water depth from 484.84 ± 118.10 kg m^{-3} in surface waters close to the glacier (station AG4) to 67.56 ± 14.01 kg m^{-3} at 30 m water depth seaward (station AG1).

4.5. SPM fluxes

We combined measurements from 2 ADCP sections to complete the N-S transect investigated along the ice-front of the Kronebreen and the Kongsvegen glaciers (Fig. 1c) to estimate water and SPM fluxes from the whole ice complex. The whole transect covered an area of 200,022 m^2 (northern section) and 223,230 m^2 (southern section) for a total of 423,252 m^2. The instantaneous water fluxes across these sections were estimated to −110.09 ± 57.63 and 740.23 ± 119.19 m^3 s^{-1} respectively. By convention, positive values indicate eastwards fluxes (i.e., towards the ice front) and negative values westwards fluxes (i.e., towards the fjord). The net water flux over the whole transect is then estimated at 630.14 ± 176.82 m^3 s^{-1}. Considering the SPM fluxes, we estimated instantaneous fluxes of −0.49 ± 0.03 and 0.02 ± 0.04 t s^{-1} across the northern and southern sections respectively. The net SPM flux over the N-S transect is then estimated at −0.48 ± 0.07 t s^{-1}. We finally estimated annual water and SPM fluxes of the Kronebreen-Kongsvegen ice complex by extrapolating our measurements over a 2-month average period corresponding to the melting period. Annual water and SPM fluxes were estimated at 3.26 ± 0.91 × 10^9 m^3 y^{-1} and -2.48 ± 0.36 × 10^6 t y^{-1}, respectively.

5. Discussion

5.1. Hydro-sedimentary processes

Inputs from tidewater glaciers play a major role in the stratification of water masses in the coastal zone during the summer melting season (Harms et al., 2007; Rajagopalan, 2012; Svendsen et al., 2002; Trusel et al., 2010). The freshwater outflow induces steep physical gradients of temperature, salinity, SPM concentrations and sedimentation along the Kongsfjorden (Hop et al., 2002; Kotwicki et al., 2004). Strong physical gradients were observed from in situ measurements close to the Kronebreen-Kongsvegen ice complex as shown from salinity, temperature, density and SPM concentrations (Fig. 4). Hydrological measurements suggested a 2-layer system with a surface layer of 20 m depth influenced by the inputs of meltwaters, and a bottom layer corresponding to fjord local waters. However, we also observed strong differences in

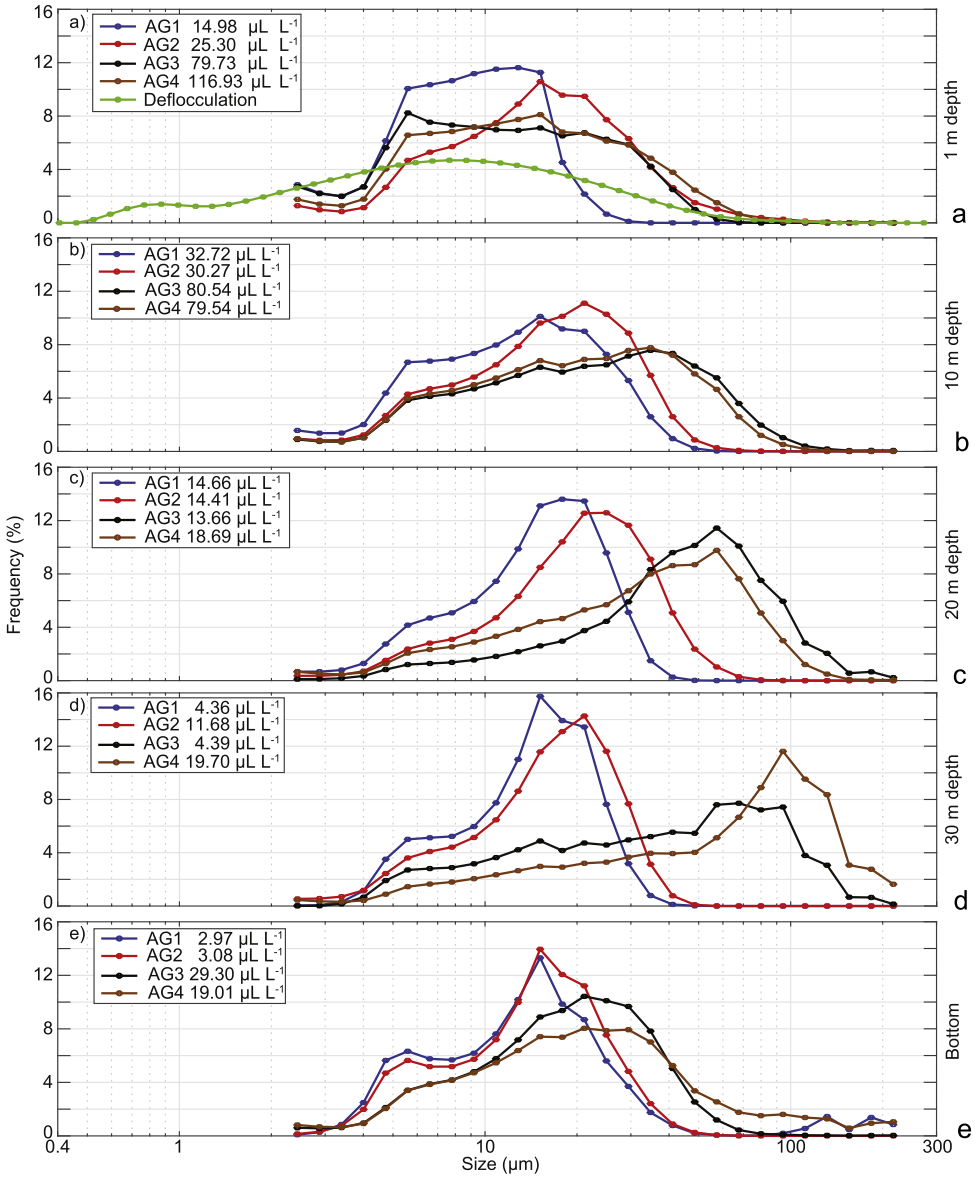

Fig. 7. Evolution of PSD from offshore towards the glacier front (station AG1 to AG4) a) at the surface (1 m), b) 10 m, c) 20 m, d) 30 m water depth and e) close to the bottom (1 meter above the bottom, mab) (e). See Fig. 1 for stations' location. In laboratory primary (deflocculated) PSD is shown in green on the top panel. (For interpretation of the references to colour in this figure legend, the reader is referred to the Web version of this article.)

hydrological parameters of the surface layer on both cross- and along-fjord directions (Fig. 4 and Fig. 6). The cross-fjord variability could be easily explained by the progressive dilution and mixing of meltwaters with adjacent fjord waters. Along the ice front, the strong gradients observed in hydrological parameters (Fig. 4b), surface hydrodynamics (Fig. 5), as well as acoustic derived SPM concentrations (Fig. 6b), allowed us to identify two meltwater sources with different characteristics (see sketches in Fig. 8). (1) In the northern part of the proximal area, strong surface currents associated with a mid-water turbid structure revealed by acoustics (Fig. 6a) suggested the presence of a particular outflow of fresh and turbid meltwater originating from a large subglacial river beneath the Kronebreen. This structure is similar to the upwelling of meltwater discharged at the base of several glaciers in fjords of Alaska (Bartholomaus et al., 2013; Syvitski, 1989), Greenland (Chauché et al., 2014) and Svalbard (Zajączkowski, 2008). These freshwaters are less dense than adjacent local waters and thus rise to the surface forming a jet. (2) In the southern part of the proximal area, close to the Kongsvegen, our measurements suggested a more conventional deltaic system with surface inputs into the fjord of fresh and turbid waters similar to riverine outflows encountered in temperate areas. Both sources contributed together to the formation of plumes of fresh and turbid meltwaters spreading beyond the inner part of the Kongsfjorden (Fig. 4). The intensity of freshwater discharges of both sources and thus of the resulting surface currents is probably dependant on the air temperature and local hydrodynamics. We also noticed that the upwelling area was characterised by warmer waters (around 3.5 °C), and more saline waters (around 32) compared to waters of the deltaic area in the south (Fig. 4). This trend could originate from the mixing at depth of basal meltwaters with adjacent fjord waters (Powell, 1990; Syvitski, 1989).

From our observations, the upwelling area introduced large amounts of sediments in the inner part of the fjord. The coarser

Table 1
Particle assemblage properties (VC_{tot} : volume concentration, [SPM]: concentration of SPM, $\Delta\rho$: effective density of SPM) at stations AG1 (offshore), AG2, AG3 and AG4 (close to the glacier front) according to the water depth.

Water depth	AG 1 (Bot. depth = 73.5 m)			AG 2 (Bot. depth = 64 m)			AG 3 (Bot. depth = 73 m)			AG 4 (Bot. depth = 74.5 m)		
	VC_{tot} ($\mu L\ L^{-1}$)	[SPM] ($mg\ L^{-1}$)	$\Delta\rho$ ($kg\ m^{-3}$)	VC_{tot} ($\mu L\ L^{-1}$)	[SPM] ($mg\ L^{-1}$)	$\Delta\rho$ ($kg\ m^{-3}$)	VC_{tot} ($\mu L\ L^{-1}$)	[SPM] ($mg\ L^{-1}$)	$\Delta\rho$ ($kg\ m^{-3}$)	VC_{tot} ($\mu L\ L^{-1}$)	[SPM] ($mg\ L^{-1}$)	$\Delta\rho$ ($kg\ m^{-3}$)
1 m	180.26 ± 7.48	30.83 ± 2.48	171.04 ± 20.84	236.66 ± 42.80	33.96 ± 5.09	143.50 ± 47.44	311.91 ± 13.22	105.04 ± 8.26	336.78 ± 40.77	241.16 ± 39.94	116.93 ± 9.12	484.84 ± 118.10
10 m	209.9 ± 15.94	42.27 ± 4.40	201.37 ± 36.25	289.7 ± 18.88	38.04 ± 3.31	131.32 ± 19.98	345.3 ± 38.04	65.63 ± 5.64	190.08 ± 37.28	288.59 ± 24.09	63.96 ± 5.61	221.63 ± 37.93
20 m	306.73 ± 11.37	28.82 ± 2.71	93.95 ± 12.30	382.23 ± 39.82	29.71 ± 3.47	77.72 ± 17.17	355.1 ± 47.20	22.15 ± 2.96	62.37 ± 16.63	265.06 ± 26.38	21.36 ± 2.19	80.60 ± 16.29
30 m	349.68 ± 34.95	23.62 ± 2.54	67.56 ± 14.01	366.43 ± 22.37	30.32 ± 2.78	82.76 ± 12.63	347.13 ± 46.23	20.45 ± 2.46	58.91 ± 14.94	300.58 ± 70.60	20.48 ± 2.99	68.15 ± 25.96
Bottom	139.70 ± 35.33	10.23 ± 1.60	73.22 ± 26.96	240.06 ± 34.23	17.13 ± 2.19	71.37 ± 19.28	308.74 ± 50.37	34.72 ± 6.89	112.44 ± 40.67	220.5 ± 46.93	23.68 ± 3.12	107.41 ± 37

fraction of SPM inputs was rapidly deposited at the seabed, building a sedimentary deposit identified below the upwelling zone from the bathymetry (Fig. 6b). Likewise, another sedimentary deposit, located 500 m south of the upwelling, certainly showed a former position of the upwelling (Trusel et al., 2010). However, the finest particles were transported to the surface through a hypopycnal plume characterised by high SPM concentrations. This plume rapidly diluted with adjacent fjord waters while rising to the surface. Low vertical velocities measured within the plume (~0.1 $m\ s^{-1}$) did not permit us to conclude that the turbid plume rose to the surface as a turbulent jet (Syvitski, 1989); instead it probably gently rose to the surface because of the buoyancy difference with surrounding waters. Acoustic measurements permitted us precisely to map and describe the upwelling area of meltwaters in front of the Kronebreen glacier. As the CTD data were not measured at the same time and at the same location as the acoustic data, we were not able to characterise the hydrological characteristics of the core of upwelled waters. Indeed, these fresh and turbid meltwaters supplied principally the surface outflow, which dominated the circulation in the fjord during melting conditions before its mixing with Atlantic waters as seen from satellite data (Fig. 1). During the export of this outflow, the surface turbid plume showed an important decrease of SPM concentrations, especially within the first kilometre from the ice front. This decrease could result from several processes. First, a strong sedimentation of the coarser sediment fraction was already observed in this area (Elverhøi et al., 1983; Svendsen et al., 2002). Authors estimated that 90% of the sediment originating from Kronebreen-Kongsvegen complex was deposited in the first 400 m from the ice front due to gravitational forces. Furthermore, SPM concentrations not only decreased with the distance from the glacier (i.e., SPM concentration was divided by 2 between the ice front and station A 2.5 km offshore, see Fig. 4a) but also decreased with water depth. This trend could be explained by two phenomena: 1) the dilution of the surface turbid plume with surrounding waters and 2) flocculation processes that could increase the settling of suspended particles.

5.2. Suspended particle dynamics

Fig. 8 synthesized all the processes involved in the SPM transport (river inputs, upwelling, gravitational sorting, and flocculation) occurring in front of a coastal glacier in an Arctic fjord. Flocculation process could be one of the most important phenomena involved in the transport of fine SPM coming from melting glaciers. While in mid-latitude regions of freshwater influence (ROFIs), flocculation processes are mainly enhanced by the organic fraction of the SPM, the SPM concentration and the salinity gradient, we present evidence here of different mechanisms responsible for flocculation processes. From our observations, the surface waters were composed of fine particles corresponding to fine silts throughout the fjord (Fig. 7a). However, measurements in underlying waters showed an increase in particle size that suggests the flocculation of the fine particles settling downwards from the surface. The initiation of this process is triggered below the surface plume within the halocline (from 10 m depth, see Fig. 4). Our results, consistent with the Syvitsky (1989) model, confirm the occurrence of the flocculation process at the glacier-ocean interface of an Arctic fjord. Lund-Hansen et al. (2010), in a similar study in an Arctic fjord-type estuary, also evidenced that suspended particles are mostly composed of flocculated material with main modes from 60 to 140 μm and primary particles of 6–10 μm. They did not find any trend in the spatial variability of floc size, however. In our study, flocculation increased with water depth as shown by the displacement of the main modes of PSD towards larger sizes from

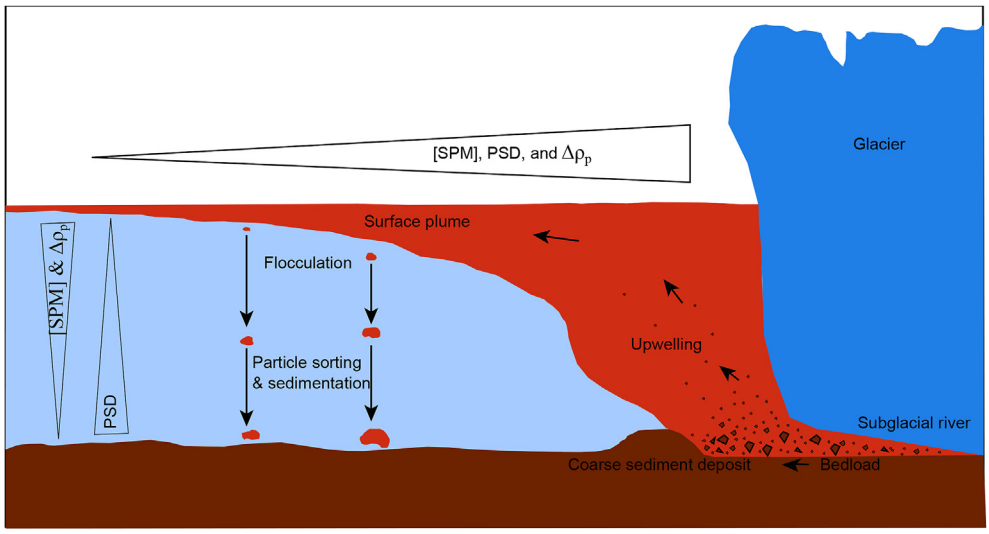

Fig. 8. Conceptual model of the particle dynamics of a typical glacial upwelling system in front of the Kronebreen glacier into the Kongsfjorden.

10 μm at the surface to 100 μm at 30 m depth close to the ice front (see station AG4 in Fig. 7b–d). Furthermore, we showed a decrease in particle size with distance from the upwelling area. This result suggests the gravitational separation of finer particles from coarser particles. The decrease in SPM concentrations with the distance from the ice front was thus induced by the sedimentation of coarser particles which are flocculated particles, while the finer fraction was transported in the surface outflow towards the exit of the fjord. However, close to the seabed, PSD were different from above water levels. Close to the bottom, PSD were characterised by finer particles corresponding to primary silty particles, which could result from direct inputs from the base of the upwelling or from sediment resuspension.

Effective densities of the particle assemblage ranged from $484.84 \pm 118.10\ kg\ m^{-3}$ in surface waters close to the glacier (station AG4) to $67.56 \pm 14.01\ kg\ m^{-3}$ at 30 m depth seaward (station AG1). These values are comparable to those estimated by Soulsby et al. (2013) in North-European estuarine environment and confirmed the phenomenon of flocculation. Indeed, a decrease of the effective density with the distance from the upwelling could be explained by the gradual loss of the larger fraction of SPM during the outflow of the surface turbid plume. Thus, PSD inside the surface plume became finer and the effective density of in-situ particles became lighter seawards (Fig. 8). The decrease of the effective density with the water depth also suggested the increase of floc proportion. However, the increase of the effective density close to the seabed of the proximal stations was linked to finer PSD. We did not find the presence of flocs close to the seabed, probably because they were rapidly exported to the bottom or towards the fjord by advection.

The presence of organic matter can enhance the formation of flocs, as demonstrated by previous studies (Ayukai and Wolanski, 1997; Many et al., 2016; Naudin et al., 1997). A previous study next to the Kronebreen ice front (Bourgeois et al., 2016) showed that 99.5% of the bottom dry sediment weight was composed of inorganic detrital materials. Nittrouer et al. (2009) also highlighted that the suspended material contained in glacial meltwaters is principally inorganic particles. They also referred to a process of coagulation instead of flocculation enhanced by Van der Waals attraction forces between fine particles. Thus, we can assume that flocculation in Kongsfjorden was principally controlled by the SPM concentration and the salinity gradient. The proximal area close to the ice front presents the most favourable conditions for the flocculation of particles, and those conditions decrease seawards.

Flocculation could also be linked to the sedimentation rates, which were high in the proximal zone ($>10\ cm\ y^{-1}$ in Bourgeois et al. (2016) and Kehrl et al. (2011)) and decreased to $0.1\ cm\ y^{-1}$ in the outer part of the fjord (Elverhøi et al., 1983, 1980). Indeed, the variation of sedimentation rates depends mainly on the intensity of flocculation within the water column, which probably increased the settling velocity of SPM. From our data, we estimated settling velocities of flocs up to $0.1\ mm\ s^{-1}$ following Stokes' law. Such settling velocity is low compared to estimates made by other authors in temperate areas who measured settling velocities of a few millimetres per second (Manning and Schoellhamer, 2013; Many et al., 2016). In our study, we probably underestimated PSD and overestimated the density. Because of high SPM concentrations encountered close to the ice front, our optical system did not accurately characterise large particles (>300 μm). Further investigations could be undertaken with specific instrumentation to better describe the whole SPM size spectra in this high turbidity area.

5.3. SPM fluxes from Arctic fjord

From our observations, we identified 2 different sources of water and SPM along the Kronebreen and Kongsvegen glaciers. We estimated that $570.70 \pm 297.35 \times 10^6\ m^3$ of water and $2.57 \pm 0.17 \times 10^6\ t$ of sediment were introduced into the fjord along the northern part of the glacier front during the 60 summer days of 2015, during which the daily average air temperature was higher than 5 °C. In this area, the upwelling area alone exported $3{,}136.83 \pm 108.03 \times 10^6\ m^3$ of water (1/3 of the total inputs to the Kongfjorden from Lefauconnier et al. (1999)) and $2.73 \pm 0.08 \times 10^6\ t$ of SPM. Along the southern part of the glacier, we estimated eastwards fluxes of $0.08 \pm 0.19 \times 10^6\ t\ y^{-1}$ of SPM and $3{,}837 \pm 297.35 \times 10^6\ m^3$ of water. Despite this, we found fluxes towards the ice front in the southern area, and we showed evidence of a surface discharge of fresh and turbid waters coming from a deltaic system in front of the Kongsvegen glacier. From our observations based on boat-mounted ADCP, we measured current and SPM concentrations below 2 m depth and we probably underestimated the surface flow. This flux toward the fjord could be explained by the general circulation of water masses close to the ice

front and was probably due to the counterbalance of the higher surface flow toward the fjord in the northern area. However, our estimate for the transect along the glacier complex of 2.48×10^6 t y^{-1} of SPM is consistent with the estimate of 2×10^6 t y^{-1} of sediments deposited in the proximal zone from Elverhøi et al. (1983). A calculated budget of SPM and freshwater throughout all the glacier front could be strongly dependent on currents and tidal conditions prevailing during the in-situ measurements as well as the meteorological conditions (i.e., waves and wind). These external forcings are fluctuating over time but they did not affect the local budget calculated next to both distinct sources (northern upwelling area and southern deltaic system). During the period of experiment, both tidal and wind conditions changed significantly. The surface outflow from the upwelling area was constant, however, and seemed to be more dependent on air temperature than on oceanic conditions. Tidal and wind conditions only affected the dynamics of the water layer located underneath the freshwater plume, but current magnitude were one order of magnitude less than in the surface layer.

Nonetheless, these local budgets give an interesting overview of two types of continental inputs into an Arctic fjord. The upwelling area is thus the major source of water and sediments from the Kronebreen-Kongsvegen ice complex to the fjord. This system contributed to more than 90% of the water and the terrestrial SPM annual fluxes from this ice complex to the fjord. The largest amount of SPM released by the Kronebreen glacier could be explained by the difference of area covered by these two glaciers (406.9 km^2 for Kronebreen vs 153.9 km^2 for Kongsvegen, according to Blaszczyk et al., 2009). Furthermore, tidewater glaciers such as the Kronebreen are more sensitive to melting because they are largely affected by local oceanographic conditions (i.e., tide, shelf water inputs, erosion by glacial rivers) that can promote both the calving and the melting of the submarine ice front area (Bennett et al., 1999; Rajagopalan, 2012).

Annual water and suspended sediment fluxes of the Kronebreen-Kongsvegen glacier are of the same order as those of a Greenland Ice Sheet sub-basin into the Kangerlussaq fjord ($1.283–1.769 \times 10^9$ m^3 and $2.009–3.502 \times 10^9$ kg respectively from Mernild and Hasholt (2009)) despite a larger drainage area (6279 km^2). In other words, the annual SPM flux estimated from the Kronebreen-Kongsvegen glacier front seems to be more important than typical small coastal rivers with similar watershed area (watershed < 5.000 km^2) located in mid-latitude areas, which discharge up to $0.48 \times 10^6 \pm 0.37$ t y^{-1} (Sadaoui et al., 2016). But, the estimate from the Kronebreen-Kongsvegen glacier front is inferior to those of medium-sized rivers in temperate areas such as the Rhône or MacKenzie Rivers that discharge $8.44 \times \pm 4.54$,10^6 t y^{-1} (Sadaoui et al., 2016) and 124×10^6 t y^{-1} (Holmes et al., 2002), respectively. However, as Svalbard is composed of about 50 fjords, the sediment budget to the Arctic ocean of this archipelago should reach those of large Arctic rivers. Glacier inputs must then be considered in the global sediment budget. We should also take into consideration the biological consequences of such inputs of terrestrial material, which should increase in the future as global warming is deeply affecting the Arctic region (Cottier et al., 2005; Overpeck, 1997). Such material is depleted in organic compounds and we assume that the petrogenic and organic fraction is old and refractory (Copard et al., 2007). Only a few opportunistic benthic organisms can survive in the vicinity of the glacier (Bourgeois et al., 2016; Wlodarska-Kowalczuk et al., 2005). Despite showing that the transport of terrestrial material through meltwater plume is currently mainly limited to the inner part of the Kongsfjorden, similar sediments, pink in colour, have been found in abundance in deep sediment cores collected on the continental shelf of western Svalbard (Rasmussen and Thomsen, 2013). These marine sediments originate from the erosion of Devonian Red Beds and their presence on the shelf reveals rapid and intense ice melt periods during Dansgaard-Oeschger warmings. This suggests that the warming climatic conditions occurring today will expand the spread of terrestrial pink sediments out of the fjord and affect habitats of benthic organisms.

6. Conclusions

During summer 2015, we investigated the characteristics and fluxes of meltwater and associated SPM inputs from the Kronebreen-Kongsvegen ice-complex and their behaviour into the Kongfjorden. Two different sources were identified: a typical glacial upwelling system along the ice front of the Kronebreen and a common deltaic system along the Konsvegen glacier. These 2 sources nourished a large turbid plume during the summer melting season that caused the inner fjord to be highly stratified. A combined set of CTD, optic and acoustic measurements permitted us to describe a glacial upwelling system and showed that (1) the upwelling is one of the major sources of water and SPM to the fjord, (2) SPM concentrations, PSD, and effective densities rapidly decreased in the surface plume from the ice front towards the fjord, (3) PSD increased from the surface plume with depth due to flocculation processes.

The upwelling probably originated from a subglacial torrential river at the base of the glacier. The coarser part of riverine particles deposited in the first kilometre from the ice front, while the finest part upwelled to the surface. In the surface plume, SPM concentrations rapidly decreased from the ice front towards the fjord due to the dilution of meltwaters within fjord waters and by dominant flocculation processes. Whereas the organic matter is one of the main parameter enhancing flocculation in temperate areas, the low organic content in SPM in the Arctic fjord suggests that high SPM concentrations and salinity gradient are the main factors controlling the flocculation in our study area. The surface plume was mainly composed of fine particles and their flocculation favoured the settling of the SPM to the bottom.

Finally, we estimated that the Kronebreen-Kongsvegen ice complex discharges about $2.48 \pm 0.36 \times 10^6$ t of sediments during the two months of melting, with a 90% contribution of the upwelling system. Arctic glaciers could thus discharge large amounts of freshwater and organic-depleted sediments to the adjacent coastal zone and could deeply affect the ecosystem by limiting light penetration and impact the benthos activities.

Acknowledgements

This work was supported by the french national programme EC2CO-Biohefect/Dril ESCOFAR. Logistics was supported by IPEV (project 1132) who provided scientific facilities, instrumentation and boat Jean Floc'h in Ny-Ålesund, Svalbard. We would like to thank the captains of the MS Teisten owned by Kings Bay AS, Norway. Kings Bay AS was also thanked for providing access to labs. We are grateful to Siegrid Debatin and Marion Maturilli for providing the meteorological data from AWIPEV station in Ny-Ålesund. We thank Nathalie Morata (ANR ECOTAB PI) for lending sediment traps. Florian Meslard was financially supported during his Master thesis by the CEFREM.

References

ACIA, 2004. Impacts of a Warming Arctic-Arctic Climate Impact Assessment. Impacts Warm. Arct.-Arct. Clim. Impact Assess. Arct. Clim. Impact Assess. Pp 144 ISBN 0521617782 Camb. UK. Camb. Univ. Press. Dec. 2004 1.

Agrawal, Y.C., Pottsmith, H.C., 2000. Instruments for particle size and settling velocity observations in sediment transport. Mar. Geol. 168, 89–114. https://doi.

org/10.1016/S0025-3227(00)00044-X.
Agrawal, Y.C., Whitmire, A., Mikkelsen, O.A., Pottsmith, H.C., 2008. Light scattering by random shaped particles and consequences on measuring suspended sediments by laser diffraction. J. Geophys. Res. 113. https://doi.org/10.1029/2007JC004403.
AMAP, 1997. Arctic Pollution Issues: a State of the Arctic Environment Report [WWW Document]. https://oaarchive.arctic-council.org/bitstream/handle/11374/923/SOAER97_03.PDF.pdf?sequence=3&isAllowed=y. (Accessed 31 March 2017).
Ayukai, T., Wolanski, E., 1997. Importance of biologically mediated removal of fine sediments from the Fly River plume, Papua New Guinea. Estuar. Coast Shelf Sci. 44, 629–639.
Bamber, J., van den Broeke, M., Ettema, J., Lenaerts, J., Rignot, E., 2012. Recent large increases in freshwater fluxes from Greenland into the North Atlantic: freshwater into the north atlantic. Geophys. Res. Lett. 39 n/a-n/a. https://doi.org/10.1029/2012GL052552.
Barnes, P.W., Reimnitz, E., Fox, D., 1982. Ice rafting of fine-grained sediment, a sorting and transport mechanism, Beaufort Sea, Alaska. J. Sediment. Res. 52.
Bartholomaus, T.C., Larsen, C.F., O'Neel, S., 2013. Does calving matter? Evidence for significant submarine melt. Earth Planet Sci. Lett. 380, 21–30. https://doi.org/10.1016/j.epsl.2013.08.014.
Bennett, M.R., Hambrey, M.J., Huddart, D., Glasser, N.F., Crawford, K., 1999. The landform and sediment assemblage produced by a tidewater glacier surge in Kongsfjorden, Svalbard. Quat. Sci. Rev. 18, 1213–1246.
Blaszczyk, M., Jania, J.A., Hagen, J.O., 2009. Tidewater glaciers of Svalbard: recent changes and estimates of calving fluxes. Pol. Polar Res. 30, 85–142.
Bourgeois, S., Kerhervé, P., Calleja, M.L., Many, G., Morata, N., 2016. Glacier inputs influence organic matter composition and prokaryotic distribution in a high Arctic fjord (Kongsfjorden, Svalbard). J. Mar. Syst. 164, 112–127. https://doi.org/10.1016/j.jmarsys.2016.08.009.
Calleja, M.L., Kerhervé, P., Bourgeois, S., Kędra, M., Leynaert, A., Devred, E., Babin, M., Morata, N., 2017. Effects of increase glacier discharge on phytoplankton bloom dynamics and pelagic geochemistry in a high Arctic fjord. Prog. Oceanogr. 159, 195–210. https://doi.org/10.1016/j.pocean.2017.07.005.
Chauché, N., Hubbard, A., Gascard, J.-C., Box, J.E., Bates, R., Koppes, M., Sole, A., Christoffersen, P., Patton, H., 2014. Ice–ocean interaction and calving front morphology at two west Greenland tidewater outlet glaciers. Cryosphere 8, 1457–1468. https://doi.org/10.5194/tc-8-1457-2014.
Copard, Y., Amiotte-Suchet, P., Di-Giovanni, C., 2007. Storage and release of fossil organic carbon related to weathering of sedimentary rocks. Earth Planet Sci. Lett. 258, 345–357. https://doi.org/10.1016/j.epsl.2007.03.048.
Cottier, F., Tverberg, V., Inall, M., Svendsen, H., Nilsen, F., Griffiths, C., 2005. Water mass modification in an Arctic fjord through cross-shelf exchange: the seasonal hydrography of Kongsfjorden, Svalbard. J. Geophys. Res. 110. https://doi.org/10.1029/2004JC002757.
Coupel, P., Jin, H.Y., Joo, M., Horner, R., Bouvet, H.A., Sicre, M.-A., Gascard, J.-C., Chen, J.F., Garçon, V., Ruiz-Pino, D., 2012. Phytoplankton distribution in unusually low sea ice cover over the Pacific Arctic. Biogeosciences 9, 4835–4850. https://doi.org/10.5194/bg-9-4835-2012.
Dagg, M., Benner, R., Lohrenz, S., Lawrence, D., 2004. Transformation of dissolved and particulate materials on continental shelves influenced by large rivers: plume processes. Continent. Shelf Res. 24, 833–858. https://doi.org/10.1016/j.csr.2004.02.003.
Elverhøi, A., Liestøi, O., Nagy, J., 1980. Glacial erosion, sedimentation and microfauna in the inner part of Kondsfjorden. Spistbergen. Geol. Geophys. Res. Svalbard Jan Mayen 33–58.
Elverhøi, A., Lønne, ølvind, Seland, R., 1983. Glaciomarine sedimentation in a modern fjord environment, Spitsbergen. Polar Res. 1, 127–150. https://doi.org/10.1111/j.1751-8369.1983.tb00697.x.
Harms, A.P., Tverberg, V., Svendsen, H., 2007. Physical qualification and quantification of the water masses in the Kongsfjorden-Krossfjorden system cross section. In: OCEANS 2007-Eur, pp. 1–6.
Hodson, A., Gurnell, A., Tranter, M., Bogen, J., Hagen, J.O., Clark, M., 1998. Suspended sediment yield and transfer processes in a small High-Arctic glacier basin, Svalbard. Hydrol. Process. 12, 73–86 https://doi.org/10.1002/(SICI)1099-1085(199801)12:1<73:AID-HYP564>3.0.CO;2-S.
Holmes, R.M., McClelland, J.W., Peterson, B.J., Shiklomanov, I.A., Shiklomanov, A.I., Zhulidov, A.V., Gordeev, V.V., Bobrovitskaya, N.N., 2002. A circumpolar perspective on fluvial sediment flux to the Arctic ocean: fluvial sediment flux to the arctic ocean. Global Biogeochem. Cycles 16, 45–1-45–14. https://doi.org/10.1029/2001GB001849.
Hop, H., Pearson, T., Hegseth, E.N., Kovacs, K.M., Wiencke, C., Kwasniewski, S., Eiane, K., Mehlum, F., Gulliksen, B., Wlodarska-Kowalczuk, M., Lydersen, C., Weslawski, J.M., Cochrane, S., Gabrielsen, G.W., Leakey, R.J.G., Lønne, O.J., Zajaczkowski, M., Falk-Petersen, S., Kendall, M., Wängberg, S.-Å., Bischof, K., Voronkov, A.Y., Kovaltchouk, N.A., Wiktor, J., Poltermann, M., Prisco, G., Papucci, C., Gerland, S., 2002. The marine ecosystem of Kongsfjorden, Svalbard. Polar Res. 21, 167–208. https://doi.org/10.1111/j.1751-8369.2002.tb00073.x.
Howe, J.A., Moreton, S.G., Morri, C., Morris, P., 2003. Multibeam bathymetry and the depositional environments of Kongsfjorden and Krossfjorden, western Spitsbergen. Svalbard. Polar Res. 22, 301–316. https://doi.org/10.1111/j.1751-8369.2003.tb00114.x.
Ingvaldsen, R., Reitan, M.B., Svendsen, H., Asplin, L., 2001. The upper layer circulation in Kongsfjorden and Krossfjorden-A complex fjord system on the west coast of Spitsbergen (scientific paper). Mem. Natl. Inst. Polar Res. - Special Issue 54, 393–407.
Ito, H., Kudoh, S., 1997. Characteristics of water in Kongsfjorden, Svalbard. Proc. NIPR Symp. Polar Meteorol. Glaciol. 11, 211–232.
Kehrl, L.M., Hawley, R.L., Powell, R.D., Brigham-Grette, J., 2011. Glacimarine sedimentation processes at Kronebreen and Kongsvegen, Svalbard. J. Glaciol. 57, 841–847.
Kotwicki, L., Szymelfenig, M., De Troch, M., Zajaczkowski, M., 2004. Distribution of meiofauna in Kongsfjorden, Spitsbergen. Polar Biol. 27, 661–669. https://doi.org/10.1007/s00300-004-0625-1.
Lefauconnier, B., Hagen, J.O., Ørbaek, J.B., Melvold, K., Isaksson, E., 1999. Glacier balance trends in the Kongsfjorden area, western Spitsbergen, Svalbard, in relation to the climate. Polar Res. 18, 307–313.
Lefauconnier, B., Hagen, J.O., Rudant, J.P., 1994. Flow speed and calving rate of Kongsbreen glacier, Svalbard, using SPOT images. Polar Res. 13, 59–65.
Lund-Hansen, L.C., Andersen, T.J., Nielsen, M.H., Pejrup, M., 2010. Suspended matter, Chl-a, CDOM, grain sizes, and optical properties in the Arctic fjord-type estuary, Kangerlussuaq, west Greenland during summer. Estuar. Coast 33, 1442–1451. https://doi.org/10.1007/s12237-010-9300-7.
Maclachlan, S.E., Howe, J.A., Vardy, M.E., 2010. Morphodynamic evolution of Kongsfjorden-Krossfjorden, Svalbard, during the late Weichselian and Holocene. Geol. Soc. Lond. Spec. Publ. 344, 195–205. https://doi.org/10.1144/SP344.14.
Manning, A.J., Schoellhamer, D.H., 2013. Factors controlling floc settling velocity along a longitudinal estuarine transect. Mar. Geol. 345, 266–280. https://doi.org/10.1016/j.margeo.2013.06.018.
Many, G., Bourrin, F., Durrieu de Madron, X., Pairaud, I., Gangloff, A., Doxaran, D., Ody, A., Verney, R., Menniti, C., Le Berre, D., Jacquet, M., 2016. Particle assemblage characterization in the rhone river ROFI. J. Mar. Syst. 157, 39–51. https://doi.org/10.1016/j.jmarsys.2015.12.010.
Maturilli, M., Herber, A., König-Langlo, G., 2013. Climatology and time series of surface meteorology in Ny-Ålesund, Svalbard. Earth Syst. Sci. Data 5, 155–163. https://doi.org/10.5194/essd-5-155-2013.
Melvold, K., Hagen, J.O., 1998. Evolution of a surge-type glacier in its quiescent phase : Kongsvegen, Spitsbergen, 1964-95. J. Glaciol. 44, 394–404.
Mernild, S.H., Hasholt, B., 2009. Observed runoff, jökulhlaups and suspended sediment load from the Greenland ice sheet at Kangerlussuaq, West Greenland, 2007 and 2008. J. Glaciol. 55, 855–858. https://doi.org/10.3189/002214309790152465.
Mikkelsen, O.A., Hill, P.S., Milligan, T.G., Chant, R.J., 2005. In situ particle size distributions and volume concentrations from a LISST-100 laser particle sizer and a digital floc camera. Continent. Shelf Res. 25, 1959–1978. https://doi.org/10.1016/j.csr.2005.07.001.
Naudin, J.J., Cauwet, G., Chrétiennot-Dinet, M.-J., Deniaux, B., Devenon, J.-L., Pauc, H., 1997. River discharge and wind influence upon particulate transfer at the land–ocean interaction: case study of the rhone river plume. Estuar. Coast Shelf Sci. 45, 303–316. https://doi.org/10.1006/ecss.1996.0190.
Nittrouer, C.A., Austin, J.A., Field, M.E., Kravitz, J.H., Syvitski, J.P., Wiberg, P.L., 2009. Continental margin Sedimentation: from Sediment Transport to Sequence Stratigraphy (Special Publication 37 of the IAS). John Wiley & Sons.
Overpeck, J., 1997. Arctic environmental change of the last four centuries. Science 278, 1251–1256. https://doi.org/10.1126/science.278.5341.1251.
Piwosz, K., Walkusz, W., Hapter, R., Wieczorek, P., Hop, H., Wiktor, J., 2009. Comparison of productivity and phytoplankton in a warm (Kongsfjorden) and a cold (Hornsund) Spitsbergen fjord in mid-summer 2002. Polar Biol. 32, 549–559. https://doi.org/10.1007/s00300-008-0549-2.
Powell, R.D., 1990. Glacimarine processes at grounding-line fans and their growth to ice-contact deltas. Geol. Soc. Lond. Spec. Publ. 53, 53–73. https://doi.org/10.1144/GSL.SP.1990.053.01.03.
Rajagopalan, D.M., 2012. Characterizing fjord oceanography Near Tidewater Glaciers Kronebreen and Kongsvegen, in Kongsfjorden, Svalbard (REU Oceanographic Data Report). Yale College.
Rasmussen, T.L., Thomsen, E., 2013. Pink marine sediments reveal rapid ice melt and Arctic meltwater discharge during Dansgaard-Oeschger warmings. Nat. Commun. 4. https://doi.org/10.1038/ncomms3849.
Sadaoui, M., Ludwig, W., Bourrin, F., Raimbault, P., 2016. Controls, budgets and variability of riverine sediment fluxes to the Gulf of Lions (NW Mediterranean Sea). J. Hydrol 540, 1002–1015. https://doi.org/10.1016/j.jhydrol.2016.07.012.
Safak, I., Allison, M.A., Sheremet, A., 2013. Floc variability under changing turbulent stresses and sediment availability on a wave energetic muddy shelf. Continent. Shelf Res. 53, 1–10. https://doi.org/10.1016/j.csr.2012.11.015.
Serreze, M.C., Barry, R.G., 2011. Processes and impacts of Arctic amplification: A research synthesis. Global Planet. Change 77, 85–96. https://doi.org/10.1016/j.gloplacha.2011.03.004.
Simpson, J., Sharples, J., 2012. Introduction to the Physical and Biological oceanography of Shelf Seas. Cambridge University Press, Cambridge ; New York.
Soulsby, R.L., Manning, A.J., Spearman, J., Whitehouse, R.J.S., 2013. Settling velocity and mass settling flux of flocculated estuarine sediments. Mar. Geol. 339, 1–12.
Svendsen, H., Beszczynska-Møller, A., Hagen, J.O., Lefauconnier, B., Tverberg, V., Gerland, S., Ørbøk, J.B., Bischof, K., Papucci, C., Zajaczkowski, M., Azzolini, R., Bruland, O., Wiencke, C., 2002. The physical environment of Kongsfjorden–Krossfjorden, an Arctic fjord system in Svalbard. Polar Res. 21. https://doi.org/10.3402/polar.v21i1.6479.
Syvitski, J.P., 1989. On the deposition of sediment within glacier-influenced fjords: oceanographic controls. Mar. Geol. 85, 301–329.
Traykovski, P., Latter, R.J., Irish, J.D., 1999. A laboratory evaluation of the laser in situ

scattering and transmissometery instrument using natural sediments. Mar. Geol. 159, 355–367.
Trusel, L.D., Powell, R., Cumpston, R., Brigham-Grette, J., 2010. Modern glacimarine processes and potential future behaviour of Kronebreen and Kongsvegen polythermal tidewater glaciers, Kongsfjorden, Svalbard. Geol. Soc. Lond. Spec. Publ. 344, 89–102.
UNESCO, 1983. Algorithms for computation of fundamental properties of seawater. Technical papers in marine science 44–53.
Wlodarska-Kowalczuk, M., Pearson, T.H., Kendall, M.A., 2005. Benthic response to chronic natural physical disturbance by glacial sedimentation in an Arctic fjord. Mar. Ecol. Prog. Ser. 303, 31–41.
Zajączkowski, M., 2008. Sediment supply and fluxes in glacial and outwash fjords, Kongsfjorden and Adventfjorden, Svalbard. Pol. Polar Res. 29, 59–72.